Decoding Lithium-Ion Dynamics: Unveiling the Role of Concentration and Local Environments in Spinel $Li_xMn_2O_4$

Yingxin Duan [a], Xiao Liu [a], Xuhong Wu [a], Zhi Yang[a], Ruiping Liu [a], Lin Xue [a], Fenglian Li [b], Jian-Li Shao [c] and Li-Chun Xu[*,a]

[a] College of Physics and Optoelectronics, Taiyuan University of Technology, Jinzhong 030600, China

[b] College of Electronic Information Engineering, Taiyuan University of Technology, Jinzhong 030600, China

[c] State Key Laboratory of Explosion Science and Technology, Beijing Institute of Technology, Beijing 100081, China

*Corresponding author.

E-mail addresses: xulichun@tyut.edu.cn

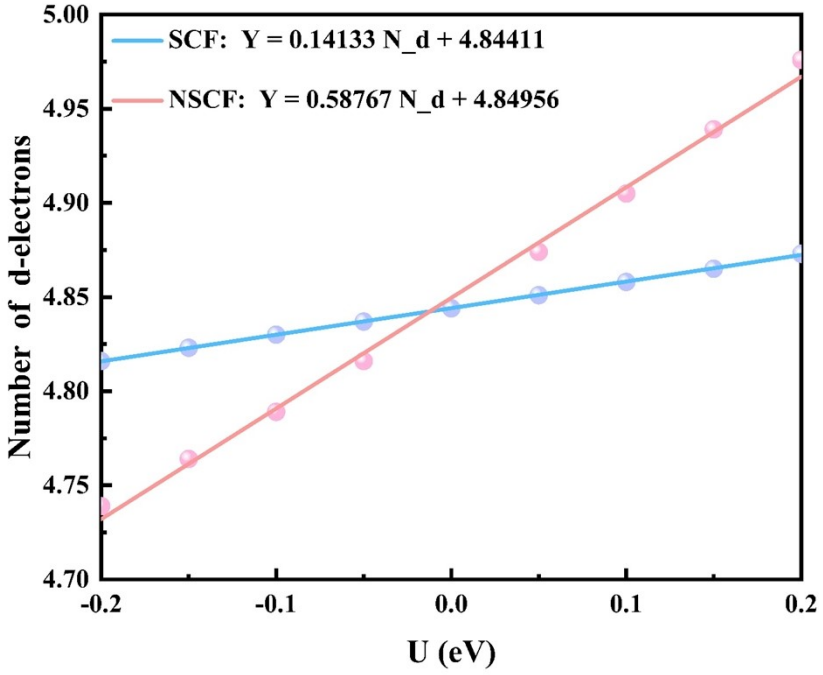

Fig. S1 Linear fit of the number of Mn *d*-electrons and the additional potential U.

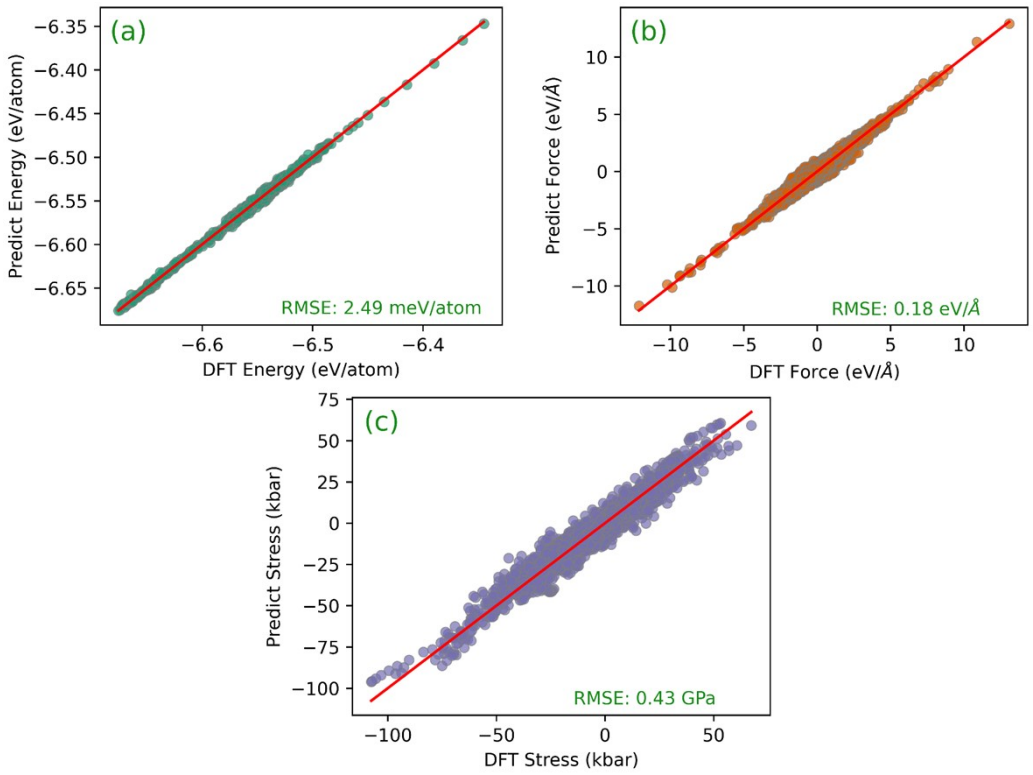

Fig. S2 The differences between the energies, forces, and stress tensors predicted by the MLFF and the DFT calculations.

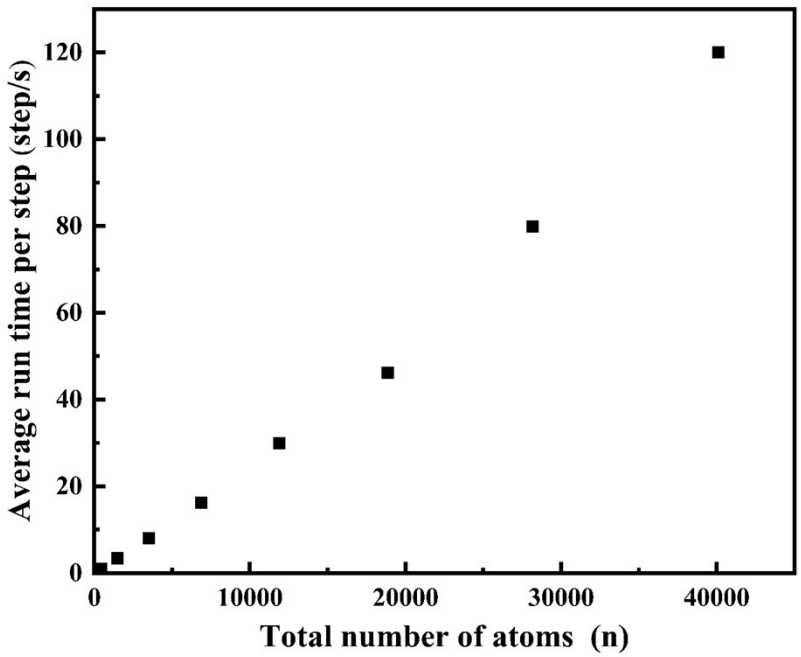

Fig. S3 Relationship between average run time per step and number of atoms.

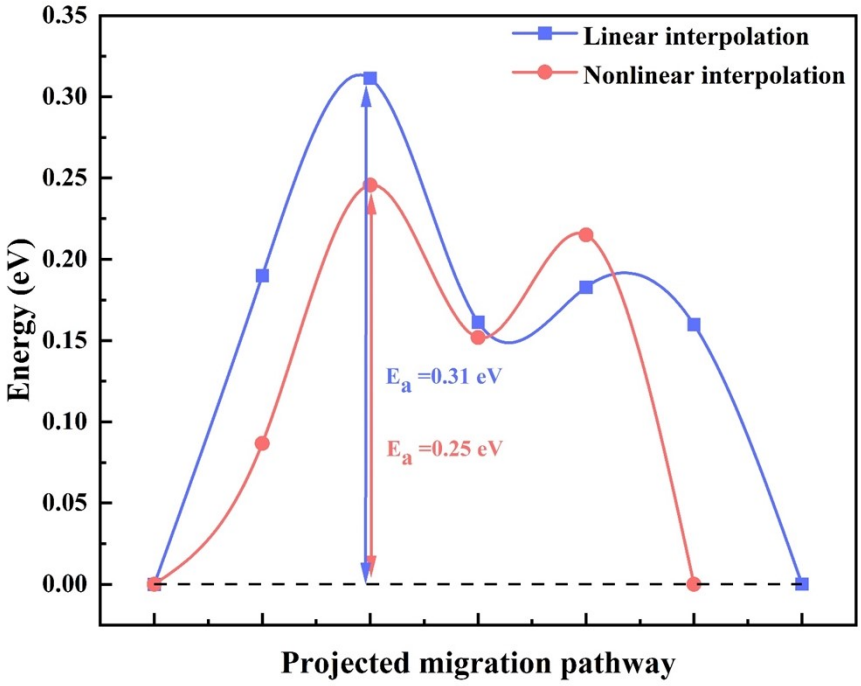

Fig. S4 Computational differences between linear and nonlinear interpolation.

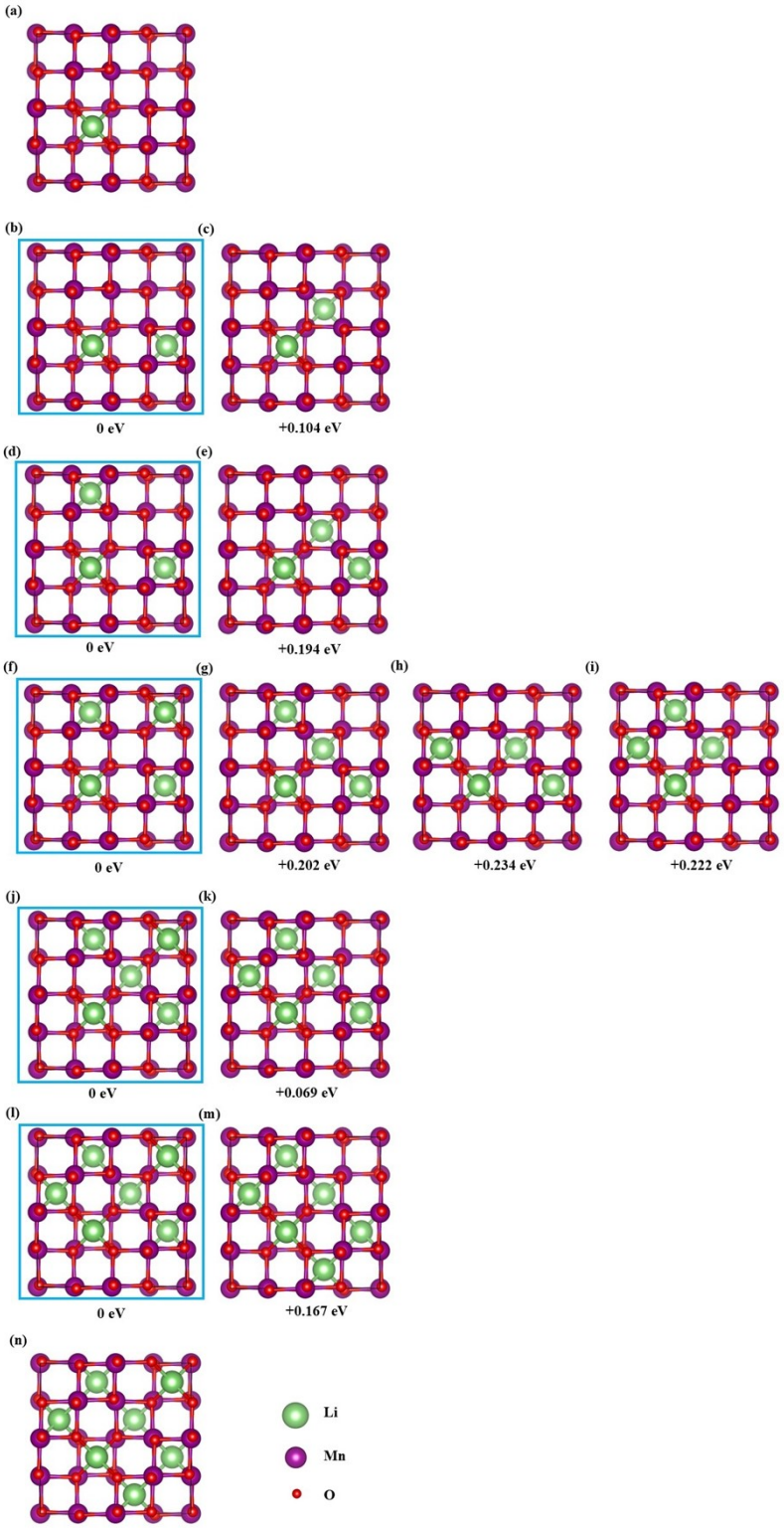

Fig. S5 Disorder Code Generated Configurations. All possible configurations at varying concentrations (x): (a) x = 0.125, (b)-(c) x = 0.250, (d)-(e) x = 0.375, (f)-(i) x = 0.500, (j)-(k) x = 0.625, (l)-(m) x = 0.750, and (n) x = 0.875. Blue boxes highlight the minimum-energy and most stable configurations for each concentration.

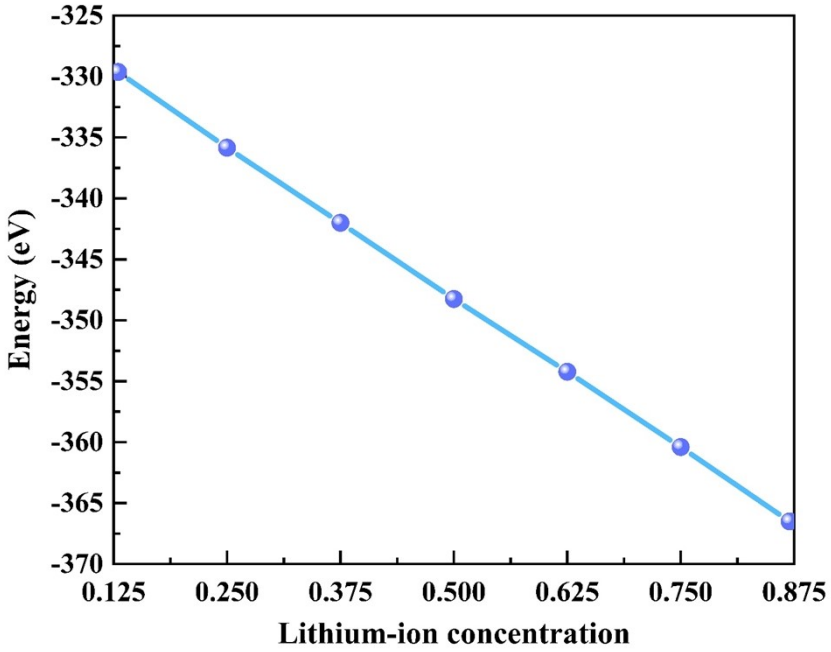

Fig. S6 The variation of the minimum energy of the lithium-ion embedding.

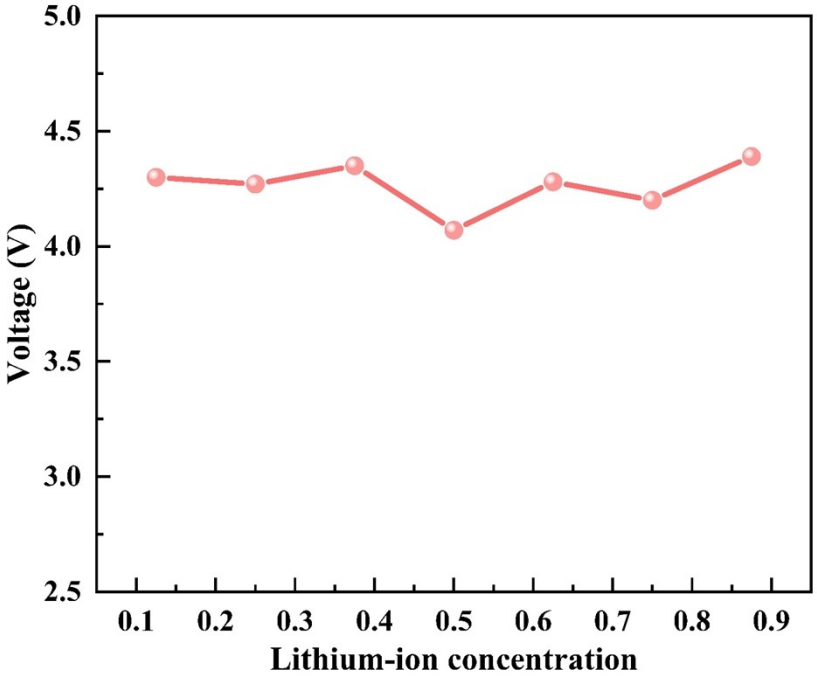

Fig. S7 The voltage platform of the $Li_xMn_2O_4$ during the charge and discharge process.

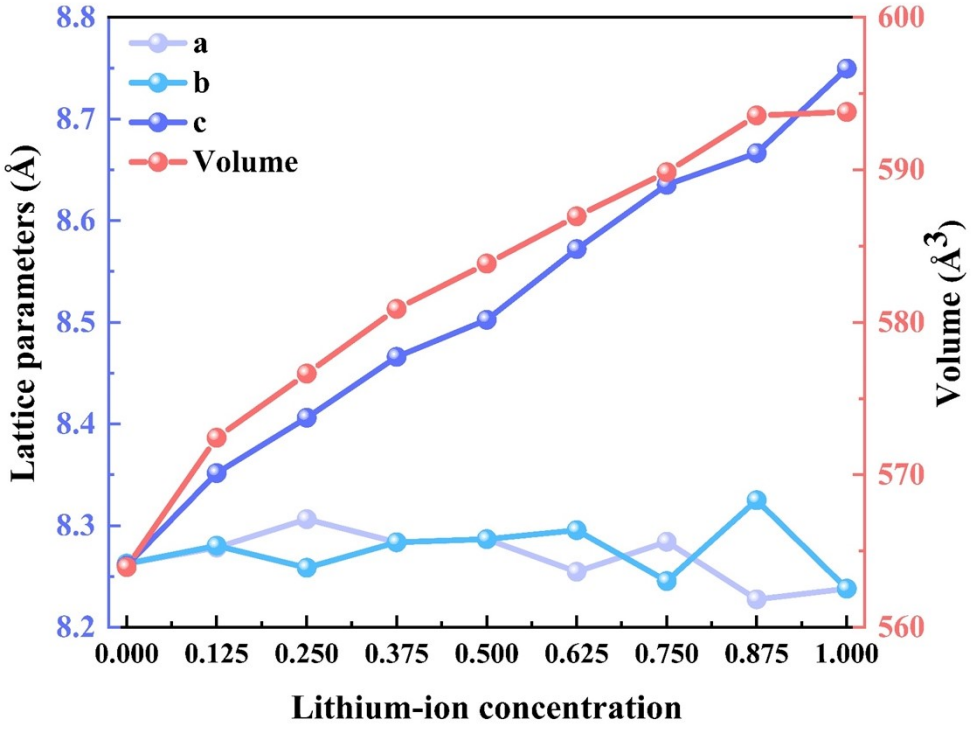

Fig. S8 Change of lattice constants and volume with concentration.

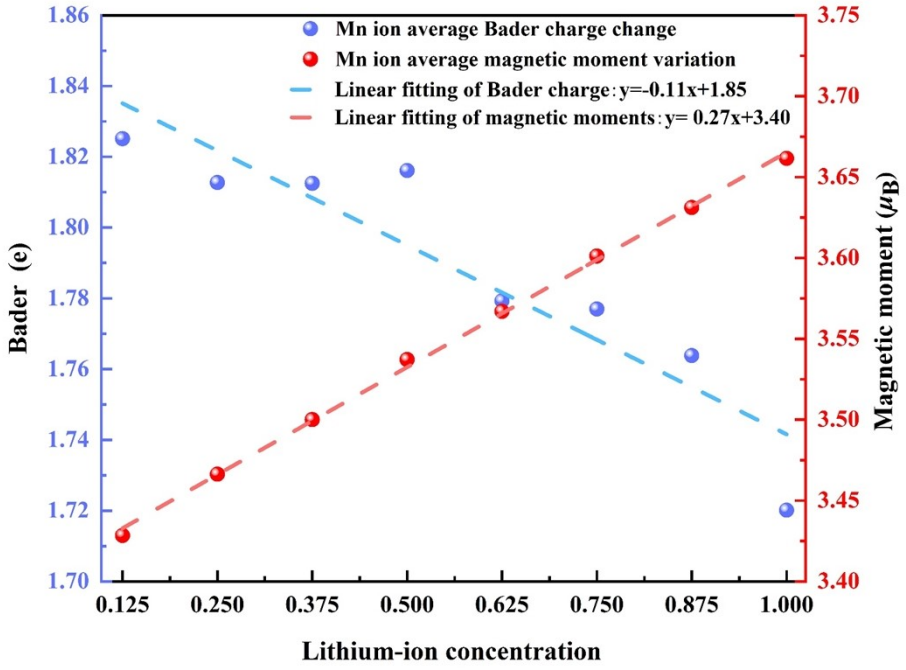

Fig. S9 Average magnetic moment and average Bader charge of Mn ion with lithium-ions concentration.

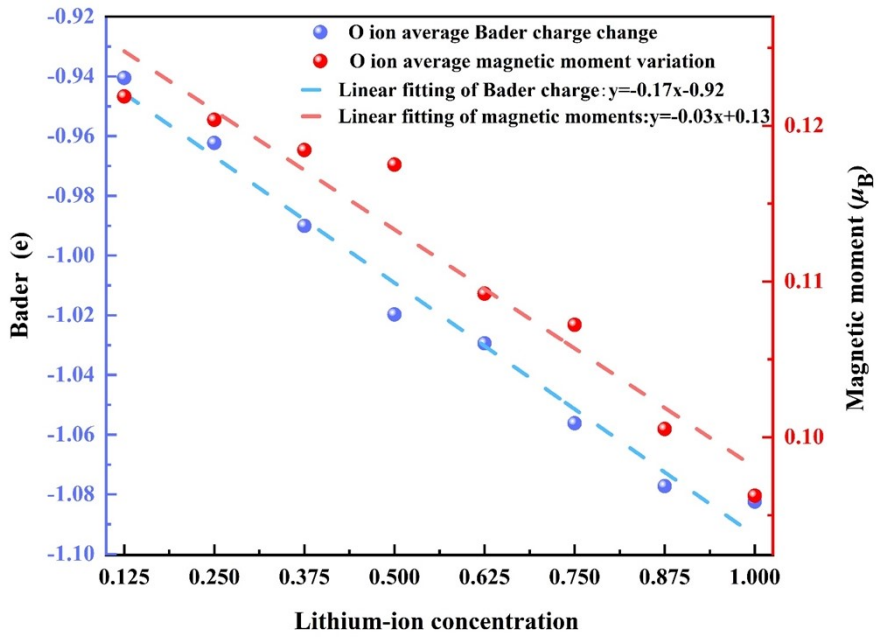

Fig. S10 Average magnetic moment and average Bader charge of O ion with lithium-ions concentration.

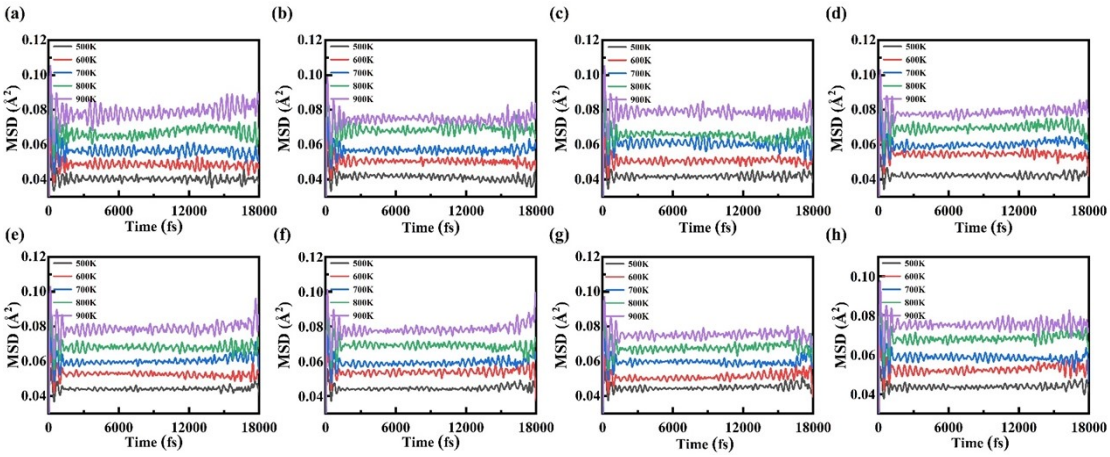

Fig. S11 The variation of MSD at different temperatures for Mn ions in $Li_xMn_2O_4$ with the concentration of (a) x=0.125, (b) x=0.250, (c) x=0.375, (d) x=0.500, (e) x=0.625, (f) x=0.750, (g) x=0.875, (h) x=1.000.

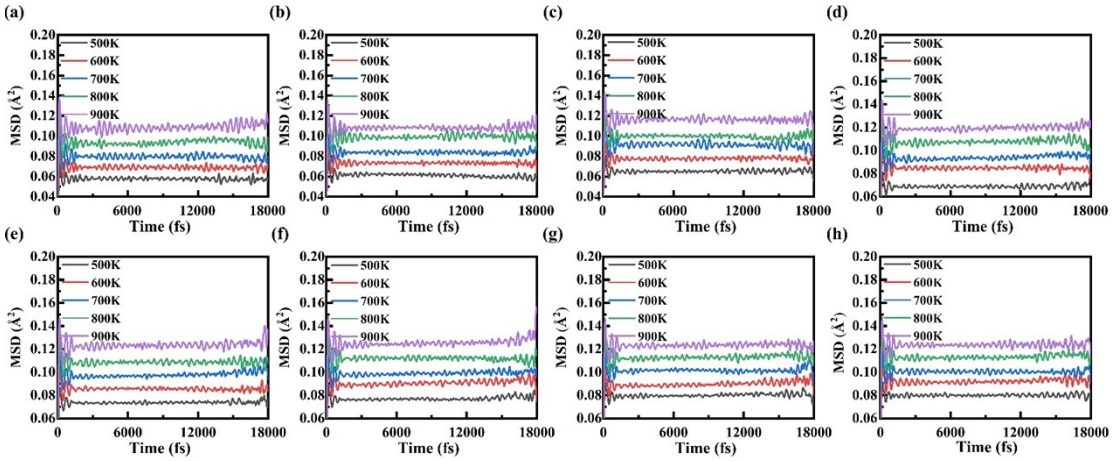

Fig. S12 The variation of MSD at different temperatures for oxygen-ions in $Li_xMn_2O_4$ with the concentration of (a) x=0.125, (b) x=0.250, (c) x=0.375, (d) x=0.500, (e) x=0.625, (f) x=0.750, (g) x=0.875, (h) x=1.000.

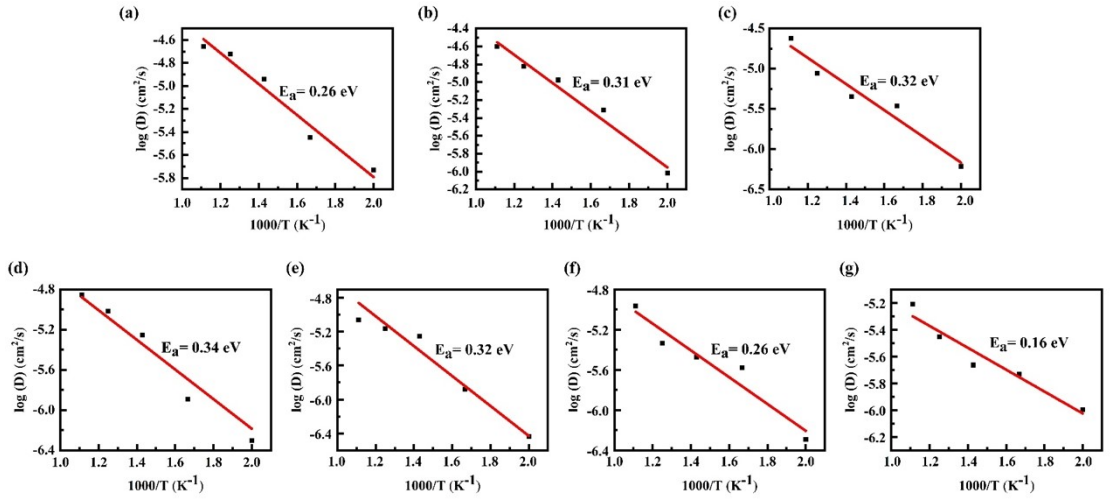

Fig. S13 A linear fit based on the Arrhenius formula between log(D) and 1000/T.

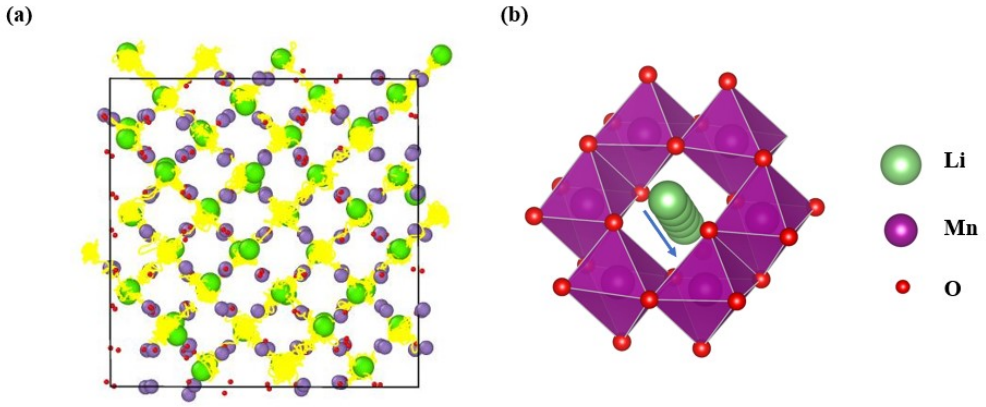

Fig. S14 (a) Diffusion trajectories (yellow track) of lithium-ions in MD and (b) the schematic diagram of diffusion path for lithium-ions (8a-16c-8a).

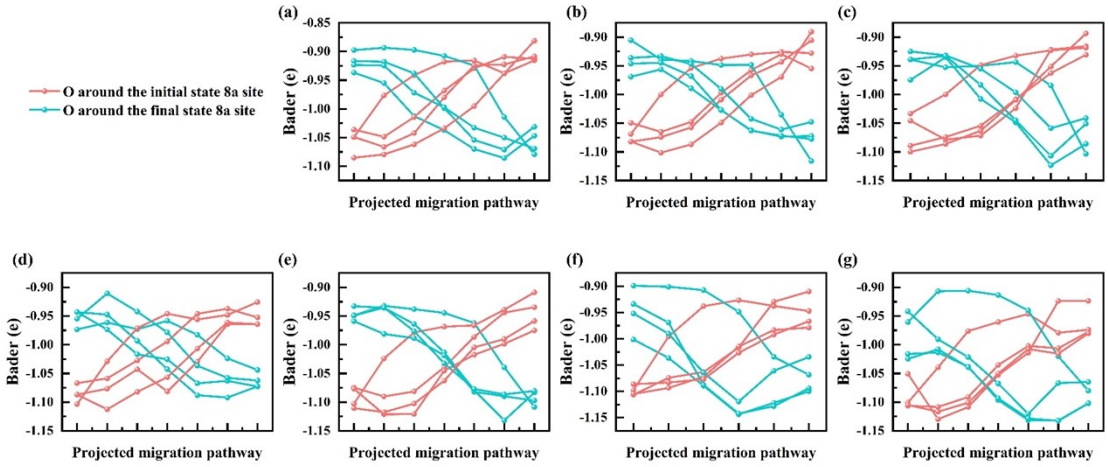

Fig. S15 The O ion around the lithium-ion diffusion at 8a site in $Li_xMn_2O_4$ is obtained Bader charge change for (a) x=0.125, (b) x=0.250, (c) x=0.375, (d) x=0.500, (e) x=0.625, (f) x=0.750, and (g) x=0.875.

Table S1. Comparison of diffusion coefficient with previous theory at 300K extrapolation.

Lithium-ion concentration	Lithium-ion diffusion coefficient (cm^2/s)	
	Previous job [Ref.40]	**This work**
x=0.125	**1.69×10^{-8}**	**3.30×10^{-8}**
x=0.500	**9.26×10^{-9}**	**2.60×10^{-9}**
x=0.875	**5.08×10^{-9}**	**8.41×10^{-8}**